The Complex Vertical Motion of Intraplate Oceanic Islands Assessed in Santiago Island, Cape Verde

F. o. O Marques, A. Hildenbrand, H. Zeyen, C. Cunha, S. s. S Victória

The complex vertical motion of intraplate oceanic islands assessed in Santiago Island, Cape Verde

F.O. Marques[a*], A. Hildenbrand[b], H. Zeyen[b], C. Cunha[c], S.S. Victória[d]

[a] *Universidade de Lisboa, Lisboa, Portugal*

[b] *GEOPS, Université Paris-Sud, CNRS, Université Paris-Saclay, 91405 Orsay, France*

[c] *Instituto Politécnico de Coimbra, Escola Superior Agrária, Coimbra, Portugal*

[d] *Universidade de Cabo Verde, Praia, Cabo Verde*

*Corresponding author. Tel.: +351 217500000; Fax: +351 217500064

E-mail address: fomarques@fc.ul.pt

Abstract

Dated paleo-sea level markers and eustatic sea level changes are necessary but not sufficient information to calculate vertical motion rates on oceanic islands. Therefore, we use a procedure in which we work progressively back in time to incorporate the more recent vertical motion rates implied by the youngest paleoshorelines into the vertical motion history of all older shorelines. Specifically, we calculate the time-averaged vertical motion rates required to explain the present-day elevations of the dated sequence of paleoshorelines on Santiago volcanic island (Cape Verde). We thus obtain a vertical motion history consisting of time-averaged vertical motion rates spanning the five intervening periods between paleoshoreline formation and the present day: (1) 5.06 to 3.29 Ma – seamount growth or island subsidence because all the rocks in this period are submarine; (2) fast uplift (ca. 0.96 mm/a) from 3.29 to 2.87 Ma, mostly responsible for putting submarine lavas

currently close to 410 m altitude; (3) relatively fast subsidence (ca. -0.11 mm/a) between 2.87 and 2.18 Ma; (4) stagnation from 2.18 to 0.811 Ma; (5) relatively fast uplift (ca. 0.14 mm/a) between 0.811 and 0 Ma. We numerically tested top-down (volcanic loading) and bottom-up (lithosphere thinning, underplating and mantle plume) mechanisms to explain the inferred vertical movements, and we conclude that volcanic loading and crustal underplating are capable of producing the observed subsidence and uplift, respectively.

Plain Language Summary

Oceanic volcanic islands experience vertical movements during their lifetime, which can be the consequence of several mechanisms like bending of the lithosphere due to the island's weight (subsidence), or horizontal intrusion of magma below the volcanic edifice (uplift). In order to discriminate among the possible mechanisms, we must correctly estimate the successive vertical displacements and motion rates. We account for eustatic sea level change and use dated paleoshorelines, working progressively back in time to incorporate the more recent vertical motion rates implied by the youngest paleoshorelines into the vertical motion history of all older shorelines, to obtain a step-by-step vertical motion history:: (1) 5.06 to 3.29 Ma – seamount growth or island subsidence because all the rocks in this period of time are submarine; (2) fast uplift (ca. 0.96 mm/a) from 3.29 to 2.87 Ma mostly responsible for putting submarine lavas currently close to 410 m altitude; (3) relatively fast subsidence (ca. -0.11 mm/a) between 2.87 and 2.18 Ma; (4) stagnation from 2.18 to 0.811 Ma; (5) relatively fast uplift (ca. 0.14 mm/a) between 0.811 and 0 Ma. From analytical and numerical modeling we conclude that volcanic loading and crustal underplating are likely mechanisms to explain the observed vertical displacements.

Keywords: uplift and subsidence rates of oceanic islands; vertical displacement in Santiago Island, Cape Verde; sea level changes; paleoshorelines; passage zones; topography response to isostasy

1. Introduction

The vertical motion of oceanic islands records the interactions between volcanic load, mantle flow and lithospheric reaction to both. An important step toward understanding the mechanisms responsible for the vertical motions in volcanic ocean islands is therefore the estimation of rates of vertical displacement. When one finds a submarine lava flow currently at 400 m altitude on an island, it means that the island was uplifted, because no specific eustatic sea level change can, by itself, explain such position. The problem is that we do not know when and how the uplift took place. As an end member, one can assume that the uplift was linear from the time of formation of the rock to present day (e.g. Ramalho et al., 2010a, c). If the rock is 4 Ma old, then 400 000 mm divided by 4,000,000 a equals 0.1 mm/a. But this assumption can be grossly wrong if geological evidence indicates that the uplift is much younger or in a much shorter period of time. If the rock is 4 Ma but uplift occurred only in the last 1Ma, then the uplift rate is 0.4 mm/a, i.e. 4 times greater than the linear estimate. If uplift occurred at 4 Ma but over a short period of time of 0.4 Ma, then the uplift rate would be 1 mm/a, i.e. one order of magnitude greater than the linear estimate. Finally, we also do not know how the submarine rock currently observed at 400 m altitude got there: was it by jerks? Or was it intercalated with periods of subsidence and/or quiescence? The unravelling of these problems is the main objective of this work. In the end, we use analytical solutions and numerical modeling to find likely mechanisms capable of explaining such vertical displacements, based on the case of Santiago Island in Cape Verde.

The calculation of vertical motion rates in an oceanic island depends critically on two

parameters: **position** of a paleosealevel marker at a given **time**. Therefore, determining the current elevation as well as the age and depth of formation of a paleoshoreline indicator are required to calculate vertical motion rates. To accomplish this fundamental objective, we looked for field evidence that allows us to determine the position of a given rock in space and time: lavas in a passage zone (transition from subaerial to submarine flow defining the paleoshoreline), preferably with in situ shallow water fossils, and which are most suitable for K-Ar dating.

Paleoshorelines record relative sea level, therefore their elevation above or below current sea level results from changes in both land and/or glacio-eustatic sea level, which has changed over time (e.g. Bintanja et al., 2005; De Boer et al., 2010; Hansen et al., 2013; Miller et al., 2005, 2011). Therefore, when analyzing vertical motions in a volcanic island, the eustatic variations of sea level must be considered.

The use of paleoshorelines and glacio-eustatic sea level curves has been used in previous works, as the methodology to assess an island's vertical motion rate (e.g. Cas and Wright, 1987; Jones, 1969; Jones and Nelson, 1970; Porebski and Gradzinski, 1990; Ramalho et al., 2013).

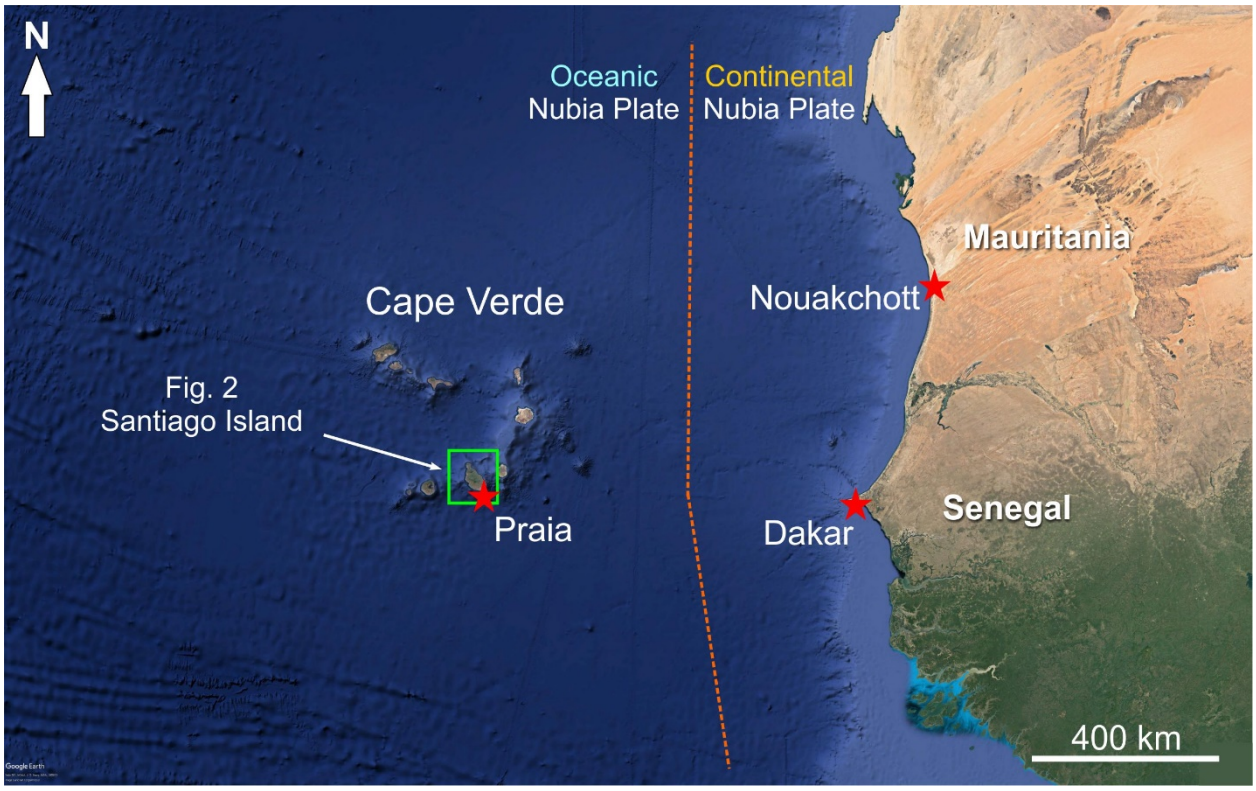

Figure 1. Annotated Google Earth image showing geographic location and tectonic setting of the Cape Verde archipelago.

The Cape Verde Archipelago comprises ten islands located about 700 km west of Dakar in Senegal (Fig. 1). They lie on Jurassic-Cretaceous seafloor, which is the basement above which the Cape Verde Rise and islands rise 2 to 8 km, respectively. Santiago Island, the target of the study reported here, is one of the islands where evidence for large vertical motion can be found. Previous work (Ramalho et al. 2010a, c) deduced a linear relationship between the vertical displacement and age of paleoshorelines on the island, implying a constant uplift rate over the past ~4 Ma. Such a relation seems incompatible with the isostatic response of the lithosphere to the complex evolution of an ocean volcanic island, which encompasses major episodes of construction and erosion/destruction (top-down forcing) as well as mantle/crustal processes like crustal underplating (bottom-up forcing).

97 The main objective was to introduce a new methodology to estimate rates of vertical motion
98 at time intervals between paleoshoreline formation, and discuss possible mechanisms responsible
99 for vertical displacement. To accomplish these objectives, we used the following methodology:
100 analysis of aerial imagery for geomorphological and geological interpretation; fieldwork to
101 recognize the major unconformities and volcanic units, to unravel the geometry and position of
102 main volcanoes, and to find the critical paleodepth markers (paleoshorelines); sampling for high-
103 precision K-Ar dating, used to calibrate the volcanic stratigraphy and to obtain the ages of the
104 critical paleodepth markers.
105
106 **2. Geological setting**
107 Santiago is the largest of the ten inhabited islands in Cape Verde. It is elongated NNW-SSE,
108 it shows rugged topography with large (km wide) and deep (up to 1 km) canyons (Fig. 2A), and
109 peaks at 1394 m at Pico da Antónia, in the center-south of the island. The northern two thirds of the
110 island are cut by deep valleys, but, in places (e.g. west of Assomada village, center of the island),
111 rugged paleotopographies can still be recognized comprising major unconformities filled with
112 younger lavas (Fig. 3).
113

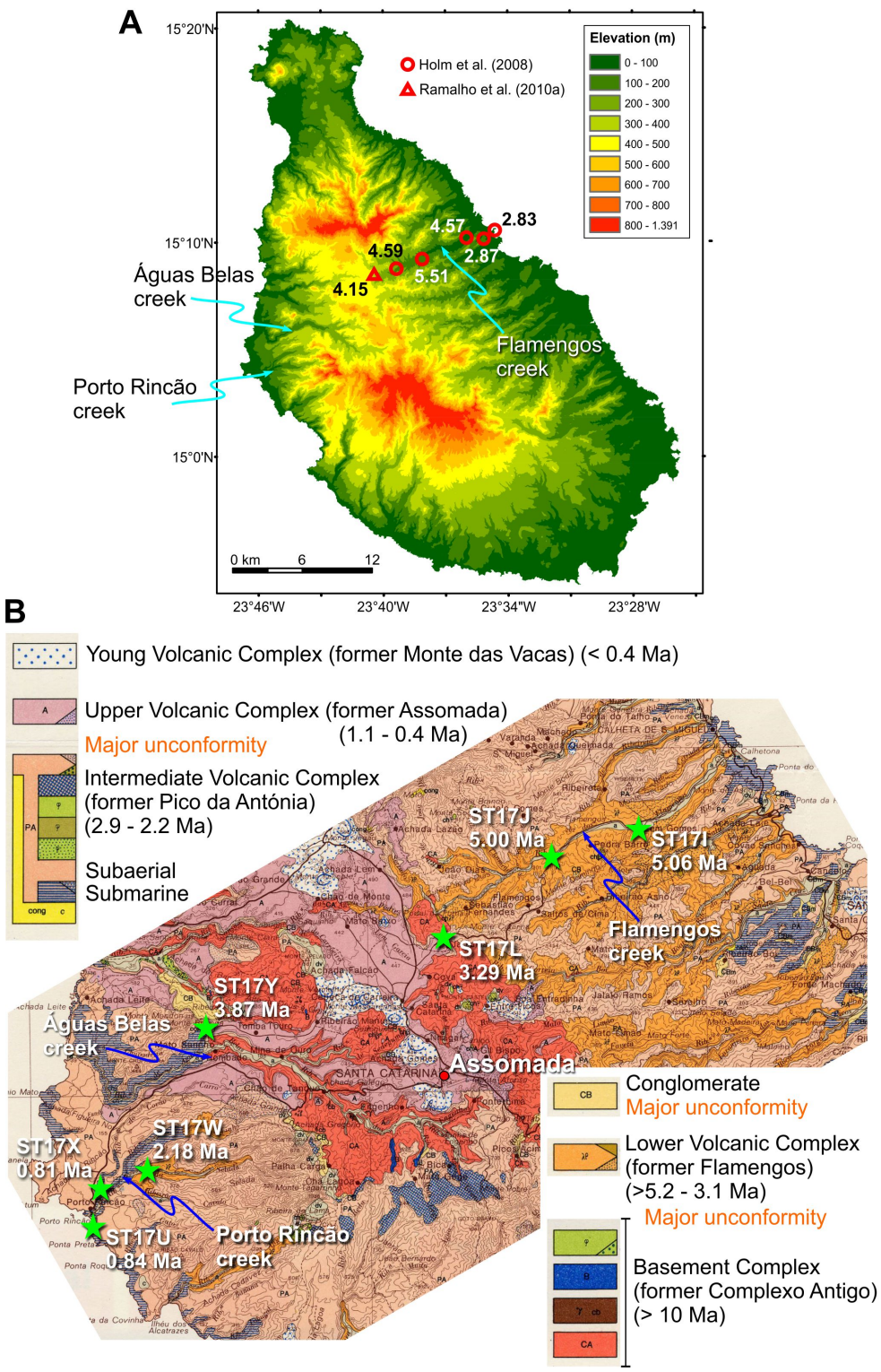

Figure 2. A – digital elevation model showing the main morphological features of Santiago, and relevant ages (in Ma) from previous studies. B – geological map of study region, (Serralheiro, 1976) with simplified volcanic stratigraphy, sample locations (green stars), sample references, and ages obtained in the present work.

The volcanic stratigraphy of the island, based on unconformity bounded stratigraphic units, is well established (Serralheiro, 1976). (Fig. 2). However, the geological map shows important inconsistencies, as suggested previously by Holm et al. (2008) and indicated here for, at least, the Porto Rincão and Águas Belas creeks. The volcanic stratigraphy of the island comprises five main volcanic complexes (Serralheiro (1976), the local names of which have no meaning to the common reader. Therefore, we introduce here more intuitive names for the different volcanic complexes, which are from bottom to top (Fig. 2B):

(1) the Basement Complex (former Complexo Antigo of Serralheiro, 1976) – deeply eroded unit mostly composed of intensely altered igneous rocks pervasively intruded by dykes and small pockets of plutonic rocks. The Basement Complex may represent an early submarine edifice (Serralheiro, 1976), but its original setting (submarine or sub-aerial) is still disputed. Biotite from a foidal gabbro, and biotite/phlogopite from carbonatites in the Basement Complex were dated at ca. 10 Ma (Bernard-Griffiths et al., 1975), which can be regarded as the minimum age for the Basement Complex because the dated rocks occur high in this unit.

(2) Lower Volcanic Complex (former Flamengos Formation) – this unit lies on the Basement Complex through a major unconformity, and is, according to current knowledge, exclusively composed of submarine lavas that outcrop from current sea level to an altitude of c. 410 m. According to Holm et al. (2008), this major submarine complex formed in a few hundred thousand years around 4.6 Ma.

(3) Intermediate Volcanic Complex (former Pico da Antónia Formation) – this unit overlies the Basement Complex and the Lower Volcanic Complex through a major unconformity, in places with a thick conglomerate, and is composed of subaerial flows that pass into submarine flows close to the current coast. This unit outcrops from current sea level to an altitude of c. 1394 m at

142 Pico da Antónia, and was dated in the range 3.3 to 2.2 Ma (Holm et al., 2008).
143 (4) Upper Volcanic Complex (former Assomada Formation) – this unit is mostly composed of thick
144 subaerial lava flows unconformably overlying all previous units. The volcanic products of this
145 unit fill valleys deeply carved in the Lower and Intermediate Volcanic Complexes, in places
146 putting the Upper Volcanic Complex directly in contact with the Basement Complex (e.g. Águas
147 Belas Creek). According to all previous work (e.g. Serralheiro, 1976; Holm et al., 2008;
148 Ramalho et al., 2010a, c), the lava flows of this later volcanic period apparently did not reach the
149 sea (no pillow lavas recognized in this unit), as can be confirmed on the geological map
150 (Serralheiro, 1976).
151 (5) Young Volcanic Complex (former Monte das Vacas Formation of Serralheiro, 1976) – this unit
152 is made of Strombolian cones lying unconformably on all previous units, and it represents the
153 latest episode of volcanism. Holm et al. (2008) considered these two younger units (UVC and
154 YVC) together as "*late volcanism*", for which they attributed an age between 1.1 and 0.7 Ma.
155

156 **3. Field data**

157 Field work carried out in the critical areas of the Flamengos (east Santiago), Porto Rincão
158 and Águas Belas (west Santiago) creeks revealed the existence of major unconformities, which
159 helped us better constrain the volcanic stratigraphy. We also found the critical outcrops comprising
160 passage zones, locally with in situ shallow water fossils (mouth of the Porto Rincão Creek), with
161 very fresh rock appropriate for reliable and precise dating by K-Ar.

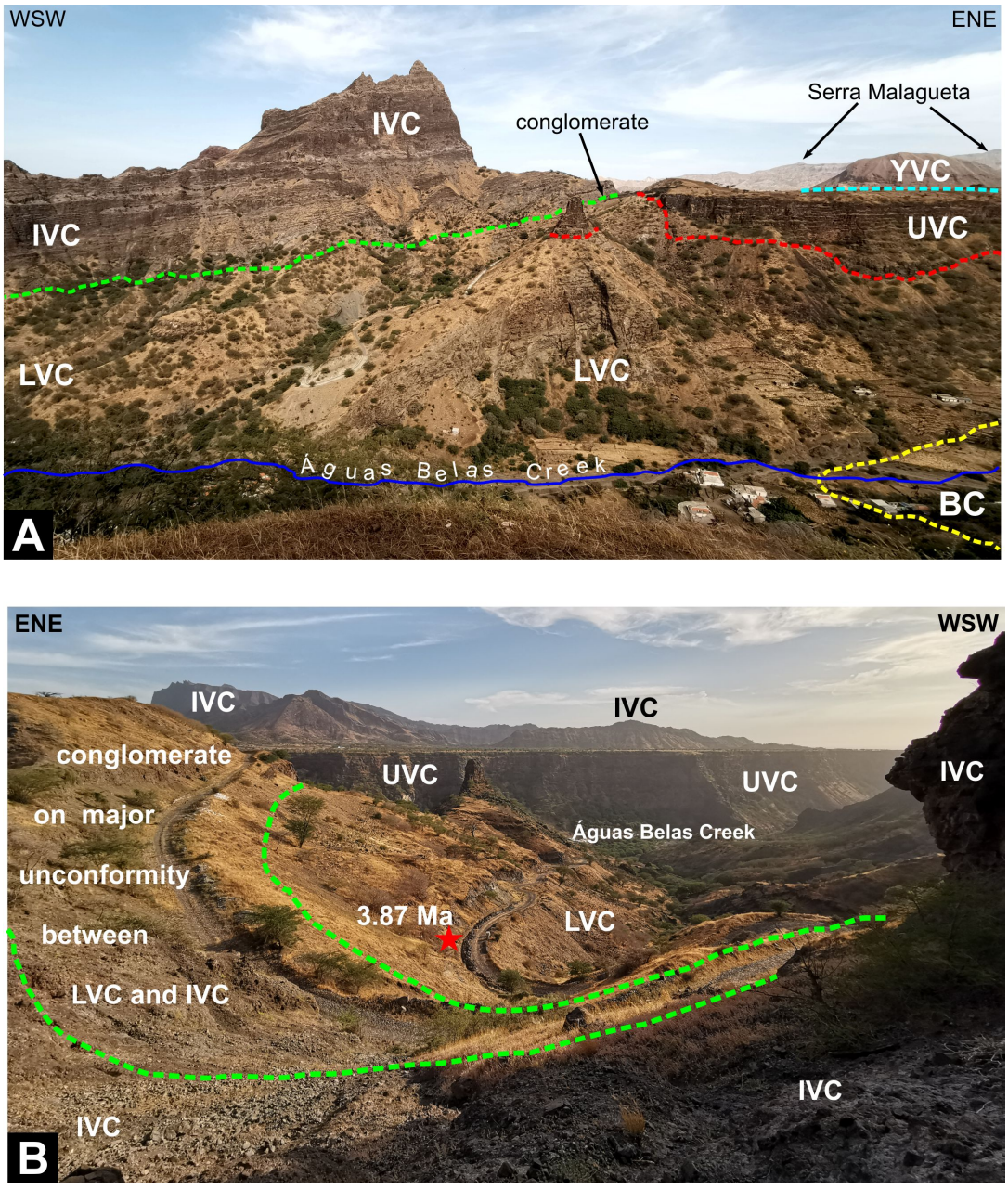

Figure 3. Annotated photographs taken to north (A) and south (B) of the Águas Belas creek with volcanic stratigraphy based on main unconformities and calibrated by K-Ar dating. In both images, especially in B, it is clear that the lava flows of the UVC fill deep valleys carved in both IVC and LVC, which stand higher than the UVC despite being older. From bottom to top: BC – Basement Complex unconformably overlain by LVC (yellow dashed line) and by UVC (out of the image); LVC – Lower Volcanic Complex (submarine flows) unconformably overlain by IVC (green dashed line) and by UVC (red dashed line); IVC – Intermediate Volcanic Complex (subaerial in the image) unconformably overlying the LVC through a thick conglomerate, and unconformably overlain by UVC; UVC – Upper Volcanic Complex made of subaerial flows filling a rugged topography carved in BC, LVC and IVC, and passing into submarine flows close to the coast (west, out of the image).

The main geology in the deep Águas Belas valley (Fig. 3) shows a major unconformity, filled with a very thick conglomerate, between the Intermediate Volcanic Complex and the underlying Lower Volcanic Complex. This is not consistent with the geological map where the underlying lavas are mapped as the submarine equivalent of the overlying Intermediate Volcanic Complex.

The critical outcrops at the mouth of the Porto Rincão Creek show clear examples of passage zones currently at ca. 43 m altitude (Supp. Fig. 1). Further upstream in the creek, we could distinguish a different unit, still made of subaerial lavas passing into submarine, but with many dykes cutting through the unit. The new ages confirmed that it is actually a different unit (cf. Fig. 4).

In the Flamengos valley, east Santiago, opposite to the Águas Belas valley, we can observe two different sequences of submarine lava flows: (1) at the mouth of the Flamengos Creek, a well preserved passage zone, ca. 20 m above current sea level, dated by Holm et al. (2008) at ca. 2.85 Ma (their samples 121367 and 121371), so confirming the geological map of Serralheiro (1976); (2) a very thick sequence (Lower Volcanic Complex, former Flamengos Formation) of gently east dipping submarine lava flows and pyroclasts up to ca. 420 m altitude, where we can observe the unconformable contact with the overlying Upper Volcanic Complex (former Assomada Formation). We could not find a passage zone in this unit, neither here nor in the Águas Belas valley, so we just collected the uppermost submarine rocks just below the conglomerates making up the major unconformity.

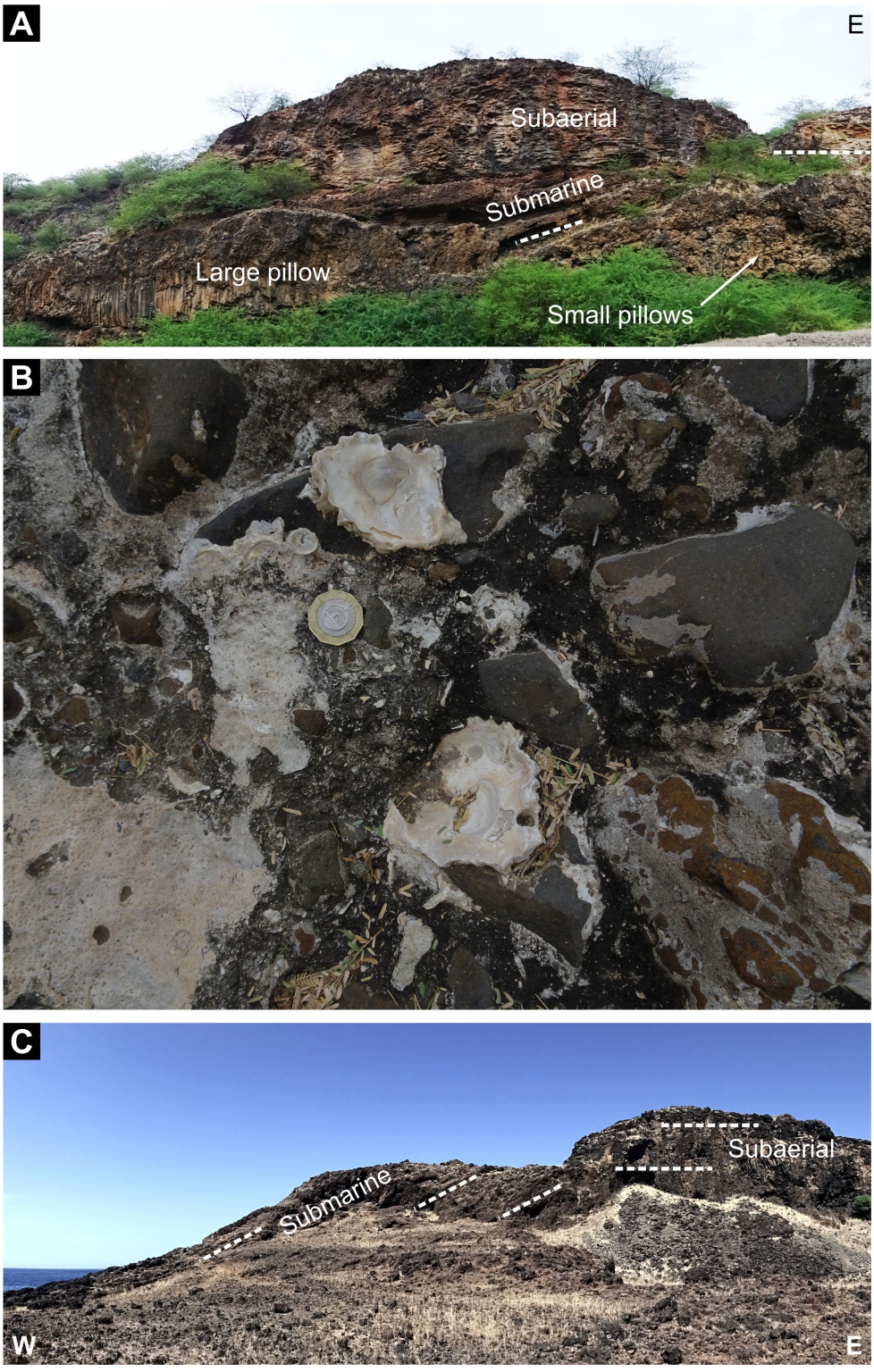

Supplementary Figure 1. Images from the Porto Rincão creek: A – passage zone with subaerial flows passing into submarine, with in situ shallow water oyster fossils, as shown in B, and sampled for geochronology; C – passage zone observed and sampled on the coast immediately south of Porto Rincão. Location of samples given in Fig. 4.

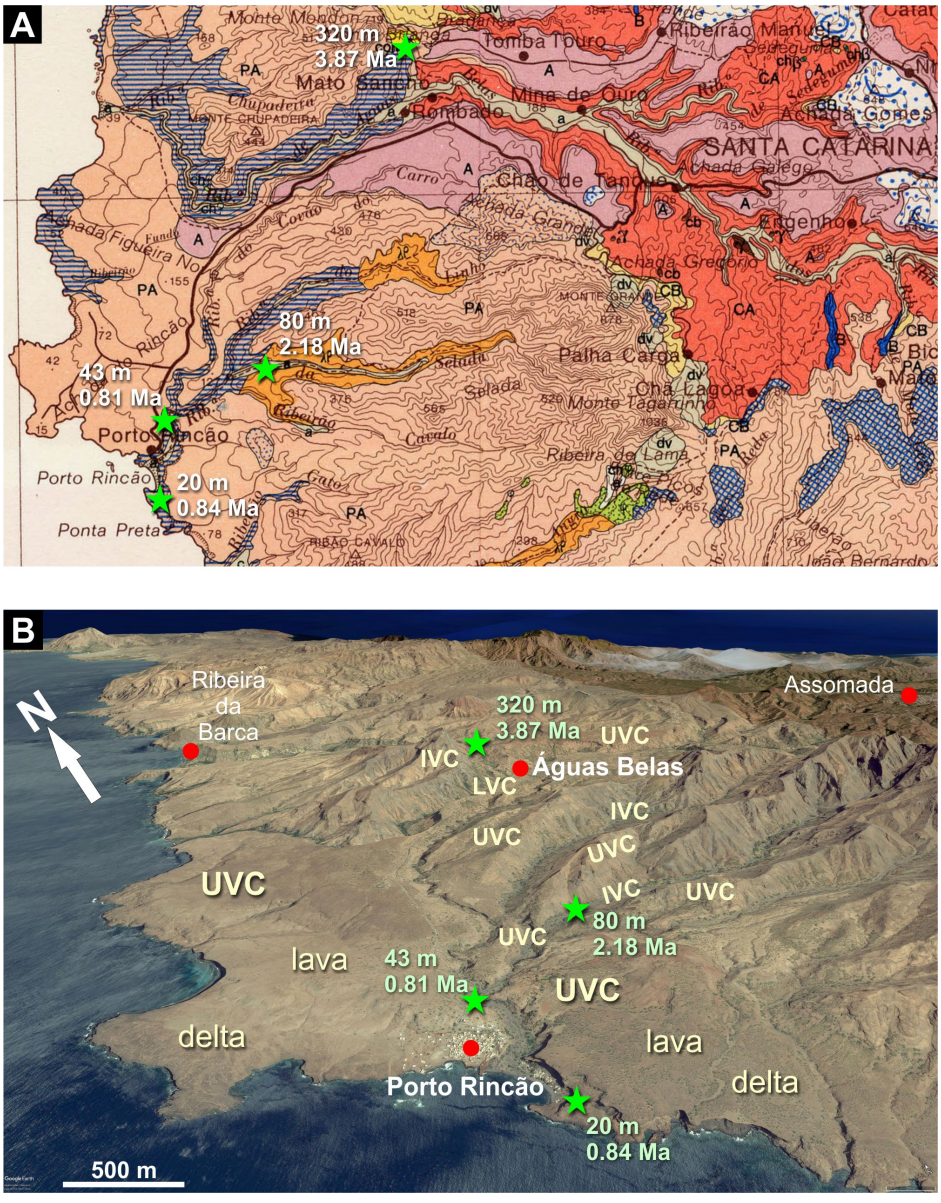

Figure 4. A – geological map of study region (Serralheiro, 1976) annotated with ages reported here. B – Perspective view of the topography, distribution of volcanic units, and their geomorphological expression. From the new ages and geomorphology, we infer that the mapped volcanic units are wrongly placed: (1) the Lower Volcanic Complex (LVC, former Flamengos Formation, orange in the geological map) in the Porto Rincão creek is actually the submarine part of the Intermediate Volcanic Complex (IVC, former Pico da Antónia Formation); (2) the submarine IVC in the Porto Rincão creek (blue horizontal stripes in the geological map) is actually the submarine part of the Upper Volcanic Complex (UVC, former Assomada Formation), which is recognized here for the first time; (3) part of the subaerial IVC (PA and peach colour in the geological map) is actually UVC, which form quite well preserved lava deltas; (4) the submarine IVC in the Águas Belas creek (blue horizontal stripes in the geological map) is actually the entirely submarine LVC.

4. K-Ar dating

4.1. Sampling strategy

We looked for passage zones and in situ shallow water fossils on pillow lavas (the critical sea level markers) and collected samples in both submarine and subaerial lavas in the Porto Rincão creek. In the absence of these ideal markers, we looked for submarine lavas and collected samples from the base (oldest) and top (youngest) of the lava pile, which was the case in the Águas Belas (western Santiago, immediately north of Porto Rincão creek) and Flamengos (eastern Santiago) creeks.

Sampling was systematically carried out on well-identified lava flows. The central massive part of the lava was extracted by means of hammers and chisels, and broken in-situ with a sledge-hammer to reach the freshest, bubble-free core of the flow and reject any vesicle-rich part. We carefully examined the rock in the field and discarded samples showing traces of weathering.

4.2. Analytical techniques – K-Ar dating on fresh separated groundmass

Thin sections of all samples were scrutinized to characterize the texture, and ensure the freshness of samples. Most samples are mafic in composition, so the volcanic groundmass was chosen for subsequent geochronological analyses. After crushing and sieving at an adequate grain size (typically 63-125 μm or 125 - 250 μm), samples were washed in dilute nitric acid and rinsed with deionized water. Magnetic separator and heavy liquids were systematically used to eliminate phenocrysts (olivine, pyroxene, plagioclase), which may carry unsuitable excess-argon, and to extract the unaltered and homogeneous fraction of the groundmass to obtain a meaningful eruption age.

Table 1. Summary of the isotopic ages reported here, with sample locations and references, geographical coordinates, and altitudes. For each sample, the mean age is obtained by weighing by the amount of radiogenic argon. Uncertainties quoted at the 1σ level.

Locality and sample reference	Latitude (N)	Longitude (W)	Altitude (m)	K (%)	40Ar* (%)	40Ar* (10^{12} at/g)	Age (Ma)	Uncertainty (Ma)
Flamengos valley (eastern Santiago)								
ST17I	15.16244	-23.60938	48	1.699	15.6	9.079	5.11	0.08
					15.5	8.889	5.00	0.08
						mean	**5.06**	**0.08**
ST17J	15.15405	-23.63730	115	1.101	27.5	5.742	4.99	0.07
					28.0	5.779	5.02	0.07
						mean	**5.00**	**0.07**
ST17L	15.13284	-23.66905	409	0.701	13.4	2.385	3.26	0.05
					10.1	2.448	3.34	0.06
						mean	**3.29**	**0.05**
Porto Rincão and Águas Belas valleys (western Santiago)								
ST17U	15.05471	-23.76369	20	1.598	19.3	1.401	0.839	0.013
					16.0	1.404	0.841	0.013
						mean	**0.840**	**0.013**
ST17X	15.06421	-23.76259	43	1.608	18.0	1.359	0.809	0.012
					29.5	1.363	0.812	0.012
						mean	**0.811**	**0.012**
ST17W	15.07013	-23.75175	80	2.042	19.1	4.611	2.16	0.03
					18.0	4.687	2.20	0.03
						mean	**2.18**	**0.03**
ST17Y	15.10868	-23.73271	324	0.542	4.3	2.163	3.82	0.10
					4.6	2.223	3.92	0.10
						mean	**3.87**	**0.10**

The samples were dated in Laboratory GEOPS (Univ. Paris-Sud, Orsay, France) with the unspiked K-Ar Cassignol-Gillot technique (Gillot and Cornette, 1986; Gillot et al., 2006), which allows the precise determination of small amounts of radiogenic argon (^{40}Ar*) and is particularly appropriate to date young volcanic rocks, including late quaternary low-K basalts and andesites (e.g., Hildenbrand and Gillot, 2006; Hildenbrand et al, 2003; 2004; 2008; 2012; 2014; 2018; Salvany et al., 2012; Germa et al., 2010, 2011; Quidelleur et al., 2008; Boulesteix et al., 2012; 2013, Costa et al., 2014; 2015; Sibrant et al., 2014, 2015a,b; Ricci et al., 2015, 2018; Silva et al., 2012, 2018; Marques et al., 2015, 2018; Bablon et al., 2018, 2019). The technique has even been extended to the last millennium with an uncertainty of only a few centuries in the case of high-K lavas (Quidelleur et al., 2001). In oceanic environments, it has also been successfully applied to date precisely submarine flows of various ages (Bonneville et al., 2006; Sibrant et al., 2015; Marques et al., 2019).

The analytical data and the new K-Ar ages are presented in Table 1, Supp. Table 1, and Figs. 2 to 5. Decay constants of Steiger and Jäger (1977) were used. Full details on the analytical procedure and performances are given elsewhere (Gillot et al., 2006). The relative uncertainty (σ_{age}) on each individual age determination is obtained as follows: $\sigma_{age}=\sqrt{(\sigma_K)^2+(\sigma_{cal})^2+(\sigma_{Ar*})^2}$, from the quadratic sum of all three independent sources of uncertainty involved in the calculation: (1) the relative uncertainty on the K-content determination (σ_K), (2) the relative uncertainty on the calibration of the ^{40}Ar signal (σ_{cal}), and (3) the relative uncertainty on the correction of the atmospheric contamination ($\sigma_{Ar*} = 0.1 / {}^{40}\text{Ar*} \times 100$), ^{40}Ar* being the radiogenic content.

(1) The relative uncertainty on K-content measurement is about 1%, from repeated measurements on standards MDO-G and ISH-G (Gillot and Cornette, 1992), and BCR-2 (Rackzec et al., 2001). For a given sample, repeated K measurements (usually twice) on distinct aliquots are achieved

until reaching an average value with a relative standard deviation (RSD) better than 1% (see supplementary Table 1).

(2) The calibration of the ^{40}Ar signal on our mass-spectrometer is obtained by systematic measurements of an air pipette, which is routinely compared to the HD-B1 biotite international standard with its recommended age of 24.21 Ma (Hess and Lippolt, 1994), recently confirmed at 24.18 ± 0.09 Ma (Schwarz and Trieloff, 2007). The relative uncertainty on the calibration, including the standard uncertainty, is 1%.

(3) The radiogenic argon content (%^{40}Ar*) is measured by comparison of the $^{40}Ar/^{36}Ar$ ratio of the sample with an air-pipette, measured under strictly similar Ar pressure conditions. This can be achieved because of the very stable analytic conditions of our mass spectrometer. The limit of detection of the radiogenic Ar content is presently of 0.1%, which allows ages as young as 2 ka to be obtained with only a few centuries uncertainty in favorable cases (Gillot et al., 2006).

For samples with low radiogenic yield (<10%), the uncertainty on the age is dominated by the uncertainty on the atmospheric contamination, and can reach several tens of %. For ^{40}Ar* higher than 10%, the uncertainty on the correction of atmospheric contamination becomes negligible, and the total age uncertainty rapidly converges towards 1.4% (i.e. $\sqrt{(1)^2 + (1)^2}$). When the individual ages overlap within their range of uncertainties, the mean age is calculated by weighting each individual age with the amount of radiogenic argon. This method is conservative, as we apply the typical relative uncertainty on K (1%) and ^{40}Ar (1%), rather than calculating the age uncertainty from duplicates of each sample, as two or three measurements are not statistically representative. Note that such approach prevents the systematic underestimation of uncertainties when duplicates yield strictly identical values.

Nine independent measurements on HD-B1 standard (Hess and Lippolt, 1994) as an

unknown in the course of the present study yielded a mean age of 24.18 ± 0.11 Ma (RSD = 0.46%, 1σ), in full agreement with the recommended value of 24.21 Ma (Hess and Lippolt, 1994), ruling out a significant potential bias linked with calibration of our mass spectrometer.

Supplementary Table 1. K-content of our samples measured by flame absorption photometry in GEOPS Laboratory (Univ. Paris-Sud, Orsay, France). For each sample, the mean is used as the final K-content for age calculation when the relative standard deviation (numbers into brackets) is better than 1%, in order to account for the total uncertainty including K-solution content and the uncertainty on BCR2 and MDO-G standards (see text).

Sample	K (%)
ST17i	1.694
	1.704
	Mean: 1.699 ± 0.007 (0.42%)
ST17J	1.099
	1.104
	Mean: 1.101 ± 0.004 (0.32%)
ST17L	0.702
	0.700
	Mean: 0.701 ± 0.001 (0.16%)
ST17U	1.598
	1.600
	1.595
	Mean: 1.598 ± 0.003 (0.17%)
ST17X	1.612
	1.599
	1.612
	Mean: 1.608 ± 0.007 (0.45%)
ST17W	2.062
	2.037
	2.026
	Mean: 2.042 ± 0.018 (0.91%)
ST17Y	0.544
	0.541
	0.542 ± 0.02 (0.40%)

Supplementary Table 2. Data necessary to calculate the rates of vertical motion. Sea level data from Miller et al. (2011).

Sample	Altitude (m)	Age (Ma)	Age uncertainty (Ma)	Relative age uncertainty (%)	Lowest sea level (m)	Highest sea level (m)	Median sea level (m)	Uncertainty on sea level (m)	Vertical displacement (m)	Uncertainty vertical displacement (m)	Relative uncertainty vertical displacement (%)
ST17X	43	0.811	0.012	1.5	-100	-44.67	-72	28	115	28	24
ST17U	20	0.840	0.013	1.5	-59	-18	-38	20	58	20	35
ST17W	80	2.18	0.03	1.5	-67	-9	-38	29	118	29	25
121367*	20	2.87	0.11	3.7	-33	6	-13	19	33	19	57
ST17Y	324	3.87	0.10	2.7	-35	-7	-21	14	345	14	4
ST17L	409	3.29	0.05	1.6	-61	-12	-36	24	445	24	5
ST17I	48	5.06	0.08	1.6	-29	5	-12	17	60	17	29
ST17J	115	5.00	0.07	1.5	-29	2.67	-13	16	128	16	12

* age data from Holm et al. (2008), with uncertainty quoted at 1^{S}

5. Rates of vertical motion

Assuming the uncertainties in both sea level and age, it is possible to estimate a mean rate of vertical movement (and its uncertainty) for each period between the age of the sample and present-day, as follows (see Supp. Table 2):

(1) From the mean K-Ar age of a sample emplaced at sea level (or close), and the available sea level dataset (Miller et al., 2011, based on $\delta^{18}O$ for the period analyzed here), we can estimate maximal, minimal and median sea levels over the period of interest. For instance, our sample ST17X yields a mean age of 811 ± 12 ka, i.e. an age in the interval 799 - 823 ka. From the dataset of Miller et al. (2011), the median sea level during this period was between -100 m and -45 m, i.e. a sea level value of -72 ± 28 m.

(2) This sea level value is subtracted from the present altitude of the sample to calculate a mean amount of vertical displacement, i.e. uplift (if positive) or subsidence (if negative). In the case of

our sample ST17X, presently at an altitude of 43 m (uncertainty on present altitude is here neglected), the estimated mean amount of uplift is thus 43-(-72) ± 28 m = 115 ± 28 m. The relative uncertainty on the amount of vertical motion is thus (28/115)*100 = 24%.

(3) The rate of vertical motion is then simply calculated by dividing the amount of vertical displacement by the mean age of the sample. The relative uncertainty on the rate of vertical motion (in %) is obtained as the sum of the relative uncertainty on the vertical displacement and the relative uncertainty on the age (very small compared to the former). For our sample ST17X, a total relative uncertainty on the rate of uplift of 25% is thus obtained. A (conservative) mean rate of uplift 0.14 ± 0.04 mm/a is thus estimated for the period between 811 ± 12 ka and present-day.

The same approach for each sample gives rates of vertical displacement over different periods and for different sectors of the island (Suppl. Table 2). The rates thus obtained are all positive suggesting at first examination that there has been only uplift during the last 5 Ma. However, a closer examination shows that the vertical motion history can be more complex. For instance, the rates obtained over the last 5 Ma (samples ST17 I and J) are one order of magnitude lower than rates obtained on the period 3.3 – 0 Ma (sample ST17L) in the same sector. This suggests a more complex history, where fast uplift may have been followed/preceded by periods with either no uplift at all, or even subsidence. It is thus necessary to use a step-by-step reconstruction to elucidate the more complex history. The new method introduced here works as follows (Figs. 5 and 6): we calculate the original position of the youngest rock unit (UVC, former Assomada), and use it to estimate the vertical displacement and the rate of vertical motion in the most recent period of time. Given that the rock is the youngest, all older rocks must follow the same motion path, which we call the anchor path (Figs. 5 and 6). Following this stage, the number of

rock units is reduced by one. And then we repeat the process using the second youngest rock unit, until we reach the oldest unit, which must follow all vertical motions of the younger units. More critically, we used paleo-shorelines (inferred from passage zones) at different age and altitude to set anchor points (Fig. 5). Given that all older rocks should show the same rate (assuming only pure vertical motion, i.e no differential movement/tilting), then the calculated path becomes an anchor path, which should be identical to all rocks (cf. blue, black and red dash-dot lines drawn parallel to the anchor green dashed line in Fig. 5). From this step onwards, all rates for older time intervals must be consistent with the anchor points and paths.

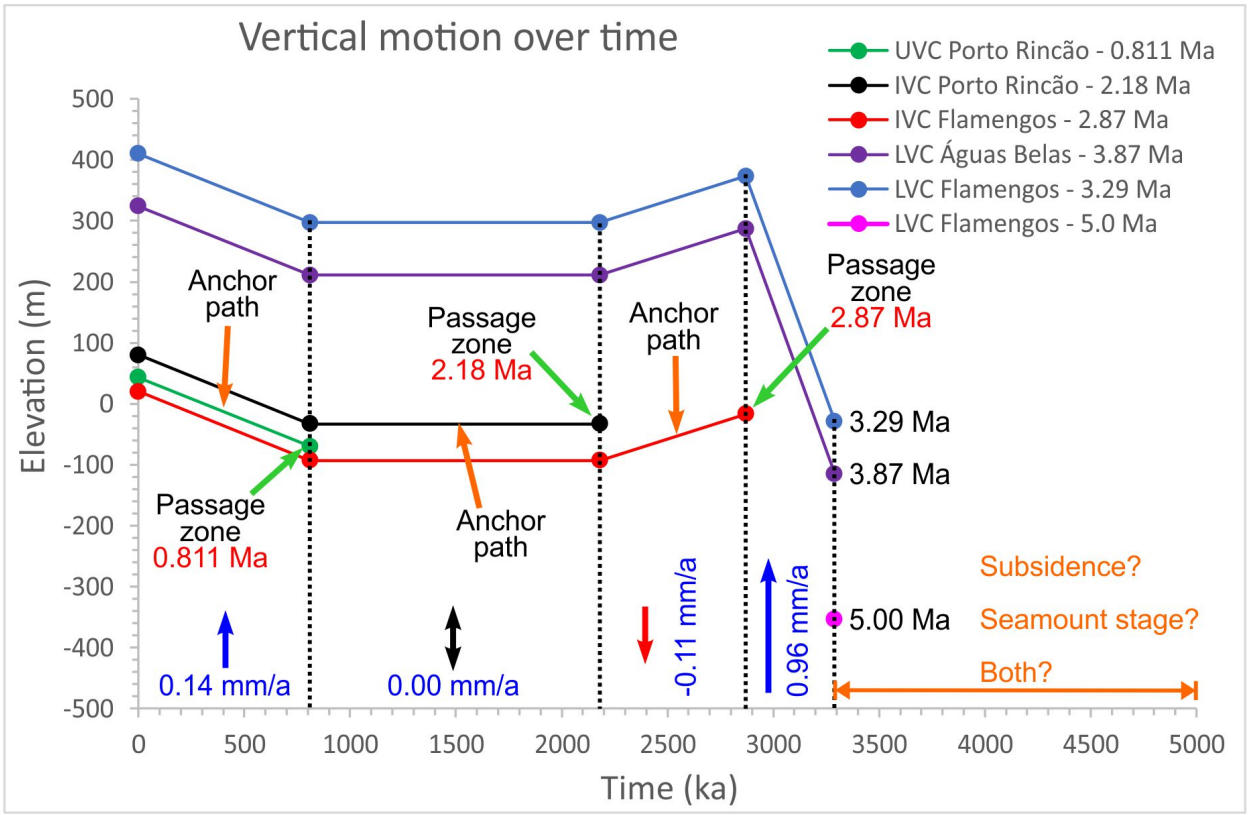

Figure 5. Sketch to show the use of anchor points (passage zones) to construct anchor paths (marked with blue arrows), which must ultimately converge to a check point. The first anchor path calculated to constrain the rates of vertical motion is the youngest (green line), because the most recent vertical motion must be identical to all units in the case of vertical motion alone. By going back in time, we obtain the paleo-positions and vertical motion rates. Note that older rocks follow a path identical to the younger rocks to guarantee that the whole island follows anchor paths. All ages were obtained in the present work, except the 2.87 Ma age reported in Holm et al. (2008).

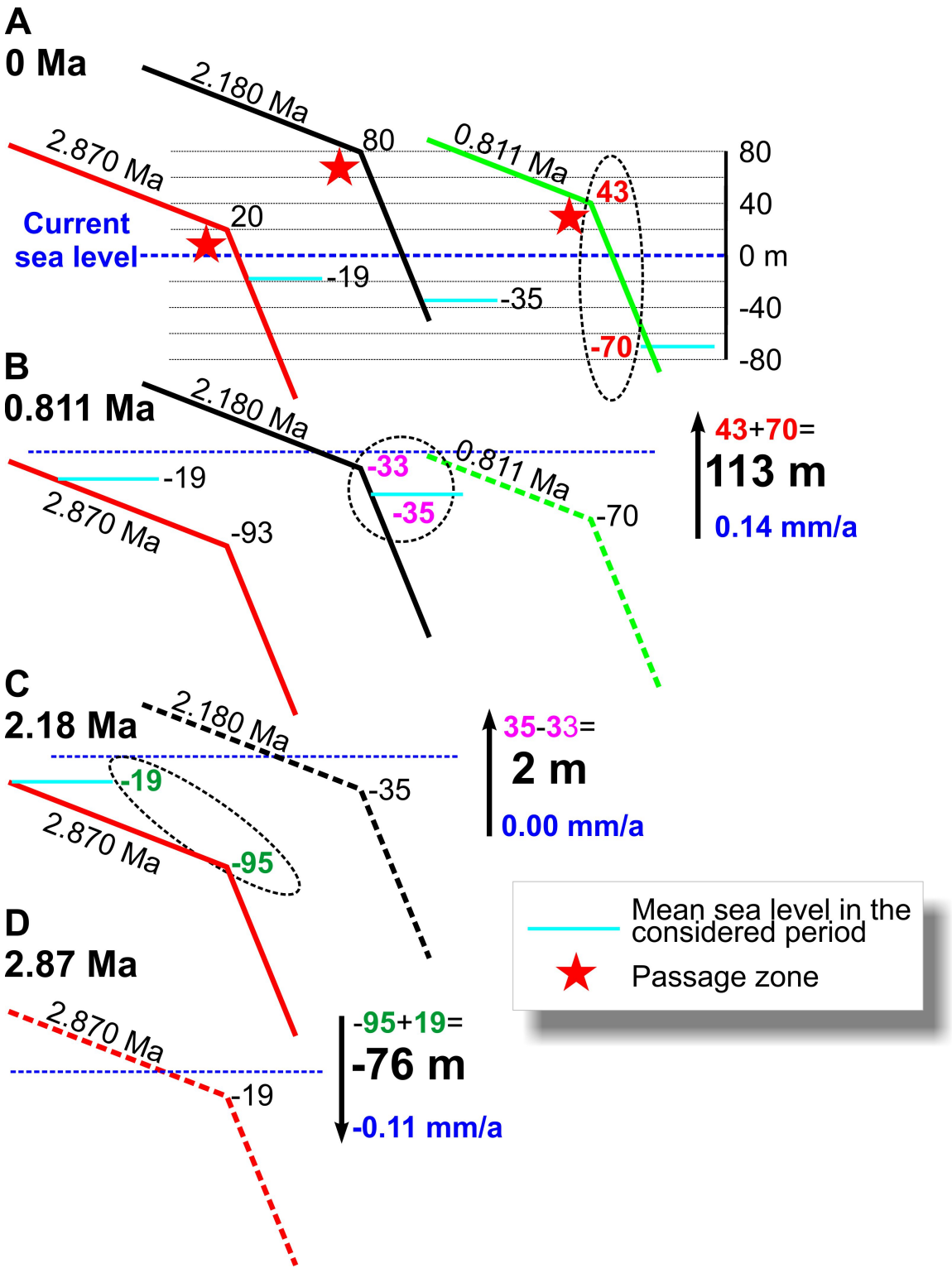

Figure 6. Sketch to illustrate the methodology introduced here to estimate vertical motion rates. The blue dashed lines represent current sea level. The sums (black bold numbers) represent vertical displacement (positive for uplift and negative for subsidence). The blue numbers represent the corresponding vertical motion rates.

Given that the effect of eustatic sea level uncertainty (in the considered time periods) on rate calculations is much greater than the effect of age error, we only consider the former in the calculations. For each period, we can use average or median sea level calculated from the dataset of Miller et al. (2011), which differ at most by only a few meters. Positive and negative vertical motion rates denote uplift and subsidence, respectively.

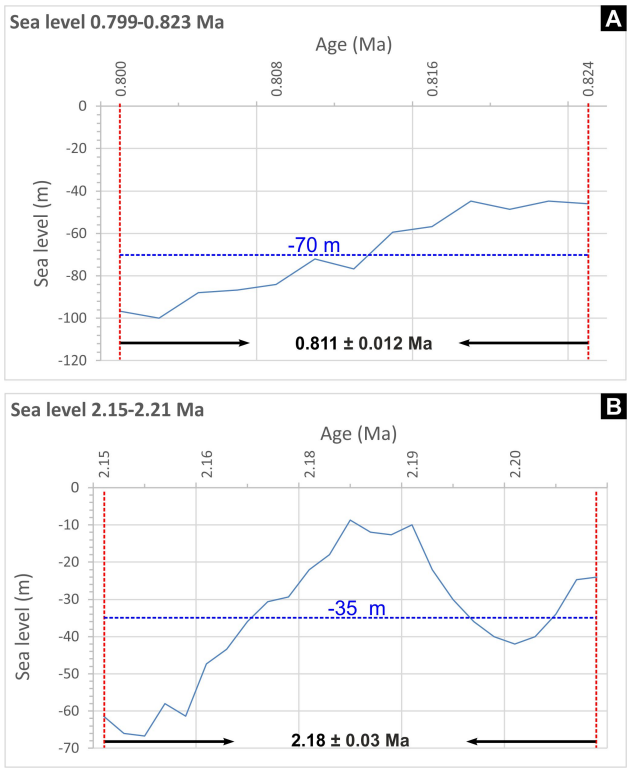

Supplementary Figure 2. Sea level curves from Miller et al. (2011) for the periods indicated in the plots. Mean sea level for each period represented by blue dashed line with respective value.

The detailed description of the procedure we used to constrauct Figures 5 and 6 can be found in the supplementary material.

Given that we could not find passage zones in the Lower Volcanic Complex at Águas Belas and Flamengos creeks, the estimated uplift rate is a minimum. At ca. 3.29 Ma, the rocks dated at 3.29, 3.87 and 5.00 Ma were at -29, -115 and -354 m depth, respectively (cf. Figs. 5 and 7), because

368 they belong to the same volcanic unit and so had to undergo the same vertical displacement, which
369 is that of the youngest rock (ca. 3.29 Ma). The highest submarine rocks of Águas Belas (ca. 324 m)
370 are not as high as the highest in the opposing Flamengos valley (ca. 410 m), but the age of the two
371 rocks is also not the same – greater in the Águas Belas valley (ca. 3.87 Ma) than in the Flamengos
372 valley (ca. 3.29 Ma), which, together with differential erosion, could justify the current difference
373 in altitude (410 -324 = 86 m).

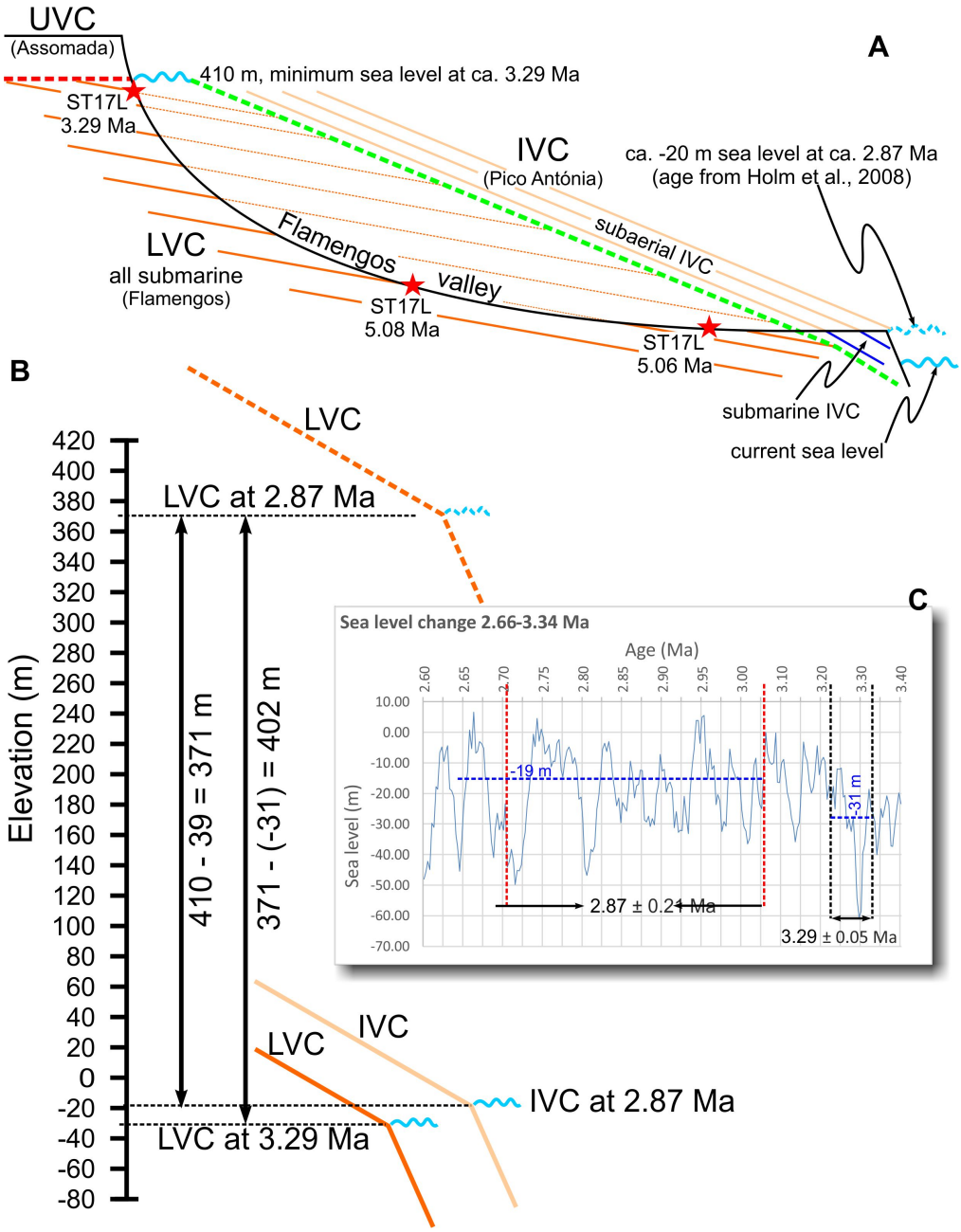

Figure 7. Sketch of the geological setting in the Flamengos valley (A) and graph (C) to illustrate how the minimum uplift rate between 3.29 and 2.87 Ma can be estimated. B – sea level curve between 2.6 and 3.2 Ma (Miller et al., 2011) to show sea level variation in the interval of the 2.87 ± 0.21 Ma age (Holm et al., 2008). The average sea level in the period is ca. -20 m, which means that the current altitude of ca. 20 m of the passage zone corresponds to sea level. LVC – Lower Volcanic Complex (former Flamengos Formation of Serralheiro, 1976); IVC – Intermediate Volcanic Complex (former Pico da Antónia Formation, which can be subaerial – pink lines, and pass into submarine – blue lines); UVC – subaerial Upper Volcanic Complex (former Assomada Formation). Red dashed line – major unconformity between LVC and UVC; green dashed line – major unconformity between LVC and IVC.

6. Discussion

6.1. New ages

From field work in the target area, geomorphological analysis and the new ages reported here (Fig. 4), we have updated and improved previous mapping of the volcanic units: (1) the Lower Volcanic Complex (former Flamengos Formation, orange in the geological map) in the Porto Rincão creek is actually the submarine part of the Intermediate Volcanic Complex (former Pico da Antónia Formation); (2) the submarine Intermediate Volcanic Complex in the Porto Rincão creek (blue horizontal stripes in the geological map) is actually the submarine part of the Upper Volcanic Complex (former Assomada Formation), which is recognized here for the first time; (3) part of the subaerial Intermediate Volcanic Complex (former Pico da Antónia, peach color in the geological map) is actually Upper Volcanic Complex, which form quite well preserved lava deltas; (4) the submarine Intermediate Volcanic Complex in the Águas Belas creek (blue horizontal stripes in the geological map) is actually the entirely submarine Lower Volcanic Complex. The recognition that the geological map is incorrect in critical places suggests that previous work based on the geological map may be erroneous.

6.2. Rates of vertical motion

We present a new methodology to deduce vertical motion histories, which can be applied to any island or coastline hosting sequences of paleoshorelines of determinate age. Here we use this methodology and new K-Ar chronostratigraphy to infer the vertical motion history of Santiago Island. We complemented the new methodology with an exercise based on state-of-the-art geochronology and a paleo sea level curve (Miller et al., 2005, 2011). Sensitivity tests indicate that the vertical displacement rates we deduce in a given interval are relatively insensitive to our choice

of eustatic sea level curve (Bintanja et al., 2005; De Boer et al., 2010; Hansen et al., 2013), and came to the conclusion that none can change our results significantly, i.e. none can change subsidence into uplift or vice-versa. In fact, we already show this when we estimate vertical displacement rates using the end-member values in a given interval.

Using the geological map of Serralheiro (1976), Ramalho et al. (2010a, c) estimated vertical motion in Santiago, but were unable to find and date passage zones, the critical criterion for an ideal marker of paleo sea level (cf. Table 4 of Ramalho et al., 2010c). They used submarine lavas at ca. 270 m altitude in the Águas Belas Valley to estimate paleo sea level at ca. 2.8 Ma, because the geological map attributes these rocks to the submarine Intermediate Volcanic Complex (former Pico da Antónia Formation). However, those submarine lavas are dated here about 1 Ma older (ca. 3.87 Ma – cf. Fig. 4), which means that they belong to the Lower Volcanic Complex (former Flamengos). Moreover, the new stratigraphy calibrated by isotopic ages indicates that the passage zone within the Intermediate Volcanic Complex (former Pico da Antónia) lies at ca. 80 m altitude in the Porto Rincão valley (immediately to the south of the Águas Belas valley), which is significantly lower than the 270 m used by Ramalho et al. (2010a, c). Therefore, the rates estimated by Ramalho et al. (2010a, c) are incorrect. Because they were unable to find passage zones, Ramalho et al. (2010a,b,c) dated outcrops of subaerial volcanic units and assumed that underlying submarine units formed at the same time and at a minimum depth below sea level equivalent to the thickness of the submarine unit. However, our fieldwork and dating show that the contact between the subaerial and submarine units is an erosional unconformity and that the subaerial volcanics are at least 2 Ma younger than the underlying submarine rocks. The rates calculated by Ramalho et al. (2010a,b,c) therefore underestimate both the minimum paleodepth (since the thickness of the eroded submarine volcanics is unknown) and the age of the paleoshoreline indicator. Given that the

whole unit is made up of submarine flows, the Lower Volcanic Complex (former Flamengos) can be interpreted in two contrasting ways: (1) the edifice was in a seamount stage, i.e. volcanic growth under sea level, therefore there is no argument in favor of any vertical motion – the older lavas simply formed deeper in the ocean; (2) the edifice was on a subaerial building stage, so that the subaerial lavas at the rim of the proto-island passed into submarine; this means that the submarine lavas formed all at similar depth in the ocean, but were gradually carried to depth by island subsidence between ca. 5 and 3.3 Ma. We do not have an answer to this question because we could neither find passage zones in the LVC, nor fossils on the pillows that could indicate depth.

Ramalho et al. (2010a, b, c) concluded for a "*general uplift trend over the last 5 Ma*" for Santiago. The use of precisely dated passage zones, at different ages (0.811, 2.18 and 2.87 Ma) and in different places on the island led us to a contrasting conclusion: instead of general uplift at a constant rate of ca. 0.092 mm/a (Ramalho et al., 2010a, b, c), our new data and procedure indicate that Santiago experienced periods of uplift, at different rates (0.95 to 0.14 mm/a), intercalated with at least one period of subsidence (-0.11 mm/a), so improving the temporal resolution of Santiago's vertical motion history.

The subsidence period here recognized corresponds to major volcanic construction, i.e. the construction of the most widespread unit in Santiago – the Intermediate Volcanic Complex (former Pico da Antónia). Subsidence may also have occurred during the deposition of the Lower Volcanic Complex, so explaining why this unit is entirely made of submarine lavas.

6.3. Mechanisms responsible for the vertical displacements of Santiago Island

Having estimated displacements and rates, we now discuss the possible mechanisms responsible for the vertical motions of Santiago Island. Here we will concentrate on two main

454 mechanisms, one top-down (island loading and unloading) and the other bottom-up (lithosphere
455 thinning, underplating, thermal mantle plume), both directly related to isostasy.

456

457 *6.3.1. Top-down: insights from isostatic calculation*

458 For the top-down mechanism, we do not have enough unloading (erosion in all its forms)
459 data to quantitatively justify the inferred uplifts. However, we have geological information enough
460 to quantitatively explain the subsidence episode in Santiago between ca. 2.9 and 2.2 Ma, which
461 corresponds to the time when the voluminous IVC was being deposited on top of a major
462 unconformity affecting both BC and LVC. These complexes underwent major erosion prior to the
463 deposition of the IVC, thus comprising one of the main unconformities whose topography peaks at
464 ca. 500 m altitude (cf. Fig. 2B). Given that the IVC peaks currently at ca. 1400 m, we can use a
465 thickness of 900 m to calculate the maximum subsidence due to loading. We can estimate the
466 isostatic effect of constructional loading by assuming Airy isostasy (i.e. the lithosphere has zero
467 strength and all loads are locally compensated) and a maximum 900 m thickness of the IVC:

468 $\varepsilon = 900 - (900*\rho_l/\rho_a) = 900 - 900*2800/3200 = 900 - 788 = 112$ m

469 where ε is the topography, ρ_l is the density of the lavas, and ρ_a is the density of the asthenosphere.
470 112 m is an upper bound calculation of the isostatic response to constructional loading, therefore
471 indicating that loading by the IVC could potentially account for the inferred ca. 80 m of subsidence
472 in this period.

473 *6.3.2. Bottom-up: insights from numerical modeling*

Different bottom-up mechanisms can be responsible for the inferred vertical movements (up to 400 m): thinning of the lithosphere by basal erosion, and/or crustal underplating, and/or arrival of a hot, low-density material at the base of the lithosphere (thermal mantle plume). We performed a set of 1-D numerical modeling tests to simulate these bottom-up mechanisms by solving the 1-D heat transport equation and calculating the uplift resulting from density variations following crustal thickening or temperature changes. We designed these modeling experiments to best reproduce the observed uplift of Santiago, assuming reasonable input parameters, to assess the viability of each mechanism.

The heat equation to be solved is the following:

$$\rho c \frac{\partial T}{\partial t} = A + k \frac{\partial^2 T}{\partial z^2} \qquad \text{Eq. 1}$$

where T is the temperature [ºC], t the time [s], z the depth [m], ρ the density [kg/m^3], c the mass heat capacity [J/(kg*K)], and k the thermal conductivity [W/(m*K)]. The boundary conditions are fixed temperatures at the top and bottom of the model domain, respectively 0 ºC and 1300 ºC (considered to be the normal asthenospheric temperature). We used standard values of k = 2.2 W/(m*K) and c = 1000 J/(kg*K) for the crust (gabbro), and k = 3 W/(m*K) and c = 1000 J/(kg*K) for the mantle (peridotite) (Robertson, 1988). Heat production was 0.2 μW/m^3 for the crust and 0.02 μW/m^3 for the mantle.

Density is related to temperature through the following equation:

$$\rho(T) = \rho(T_0) \cdot \left(1 - \alpha(T - T_0)\right) \qquad \text{Eq. 2}$$

where ρ is density [kg/m^3], α the thermal expansion coefficient [1/K], and T_0 a reference temperature at which density is ρ_0. This reference temperature is taken as 0 ºC for crustal materials

and 1300 ºC for the mantle. The thermal expansion coefficient is taken as $3.5*10^{-5}$ K^{-1} for all materials (Afonso et al., 2005). As reference density we used ρ_0 =2800 kg/m^3 for the crust and 3200 kg/m^3 for the mantle.

Several works have investigated the nature and properties of the lithosphere in the Cape Verde Swell (Ali et al., 2013; Carvalho et al., 2019; Dash et al., 1976; Hellfrich et al., 2010; Lodge and Helffrich, 2006; McNuttt, 1988; Pim et al., 2008; Vinnik et al., 2012; Wilson et al., 2010, 2013). Fundamental for the modeling are the thicknesses suggested in those works for the lithosphere and the oceanic crust, which vary from 60 km (Carvalho et al. (2019) to 100 km (Lodge and Helffrich, 2006) for the former, and from 7 km (e.g. Pim et al., 2008; Wilson et al., 2010) to 15 km for the latter (Dash et al., 1976). Therefore, we tested initial lithosphere configurations with crustal thicknesses of 7 km and 15 km, and lithosphere thickness of 80 and 100 km. Topography was calculated assuming local isostatic equilibrium using the following equation (Lachenbruch and Morgan, 1990):

$$\varepsilon = \frac{\rho_a}{\rho_a - \rho_w}\left(\frac{\rho_a - \rho_L}{\rho_a} H + \varepsilon_0\right) \quad \text{Eq. 3}$$

where ε is the topography [m], ρ_a the asthenospheric density (3200 kg/m^3), ρ_L the average lithospheric density, ρ_W the density of sea water (1030 kg/m^3), H the thickness of the lithosphere [m], and ε_0 the reference topography of an unloaded asthenosphere (-2400 m).

In the results presented below, the beginning of the calculations corresponds to 3.3 Ma ago, because this is the age of the first recognized major uplift. We present for the different models 2 to 3 calculations in order to show that different initial configurations combined with different structural modifications can explain the uplift.

516

517 *Model 1: Lithospheric thinning*

518 The temperature at the initial depth (80 or100 km) is maintained constant at 1300 ºC during
519 the whole calculation. Between 0 and 0.4 Ma in the simulation (3.3 to 2.9 Ma in nature), the base of
520 the lithosphere rises from 100 km to 60 km in steps of 5 km/0.05 Ma (blue line in Fig. 8A) or from
521 80 to 44 km in steps of 4 km/0.05 Ma (orange line in Fig. 8A), resulting in a total topographic uplift
522 of ca. 470 m. From 0.4 to 2.5 Ma (2.9 to 0.8 Ma in nature), the temperature relaxes, and the
523 lithosphere thickens slowly, resulting in a subsidence of 50 m. At 2.5 Ma (0.8 Ma in nature), a new
524 pulse of lithosphere heating is simulated by thinning the lithosphere again to 60 km / 44 km, and
525 maintaining the base of the lithosphere (i.e. a temperature of 1300 ºC) at this depth until 3.3 Ma (0
526 Ma in nature), which results in another uplift of ca. 200 m. The topography rises higher than at 0.4
527 Ma because the crust has meanwhile been heated as well. Both models give very similar results.

528

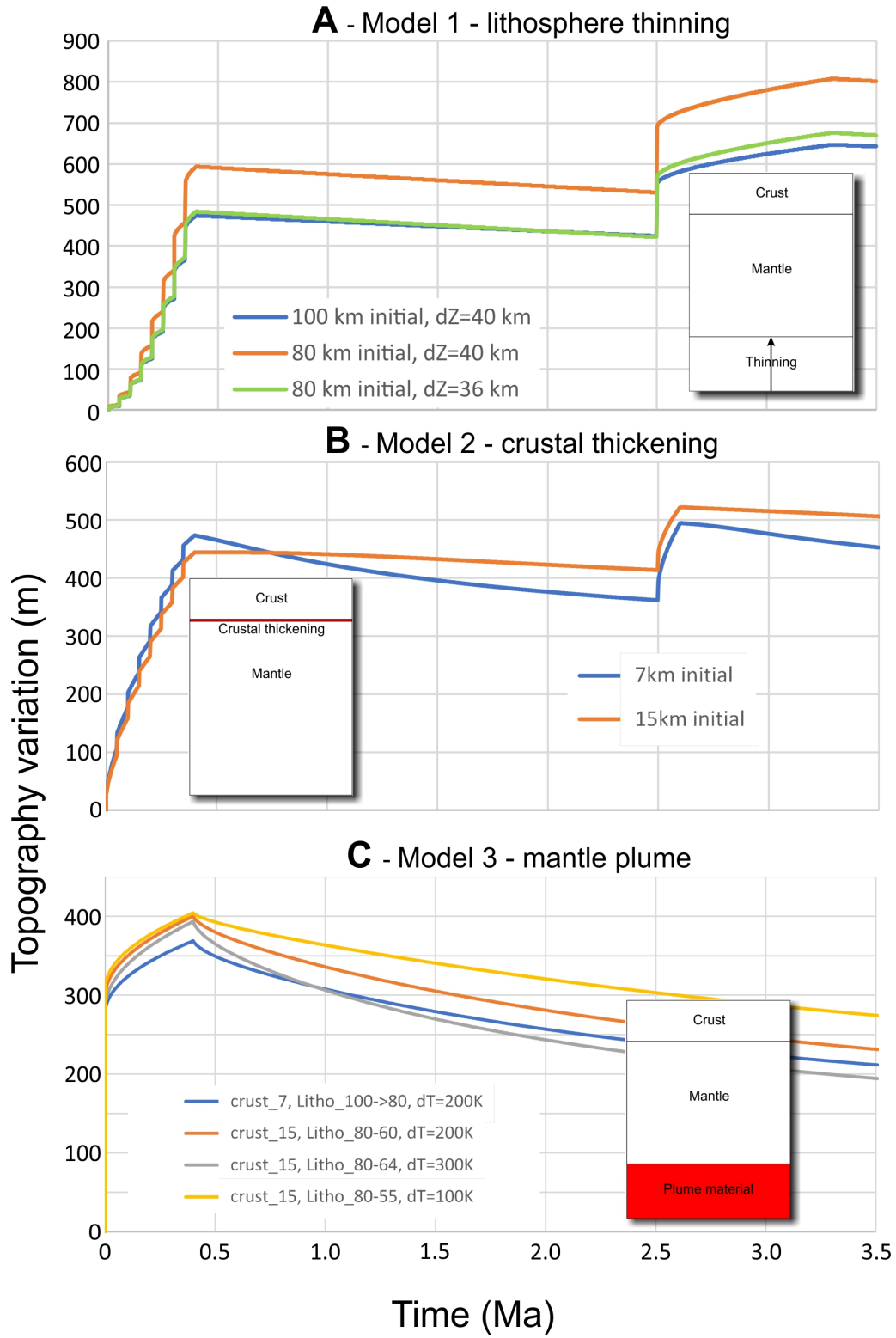

529

530 *Figure 8. Numerical modeling of the topography variation over time resulting from the Airy*
531 *isostatic response to (A) lithospheric thinning as specified in Model 1, (B) underplating as specified*
532 *in Model 2, and (C) excess buoyancy associated with a mantle plume as specified in Model 3.*

Model 2: Crustal thickening (underplating)

The crust thickens by a total of 800 m (from 7 to 7.8 km, blue line in Fig. 8B, and from 15 to 15.8 km, orange line in Fig. 8B) between 0 and 0.4 Ma (3.3 to 2.9 Ma in nature). Material arrives at 1100 °C, the typical temperature of a basaltic magma, its temperature is maintained constant until 0.4 Ma (2.9 Ma in nature) to simulate a constant supply and heating of the surrounding layers during the whole process. This results in a topographic uplift of 460 m. After 0.4 Ma (2.9 Ma in nature), the temperature relaxes and topography decreases slightly. At 2.5 Ma (0.8 Ma in nature), another pulse of thickening of 100 m (7.8 to 7.9 km) is simulated, again with a temperature of 1100 °C that is maintained during 0.1 Ma. After 0.8 Ma (at 3.3 Ma = 0 Ma in nature), it results in an uplift of 100 m, including the partial temperature relaxation between 2.6 and 3.3 Ma (0.7 to 0 Ma in nature). The effect of relaxation is stronger for the initially thinner crust, which, when taking into account the observation of roughly stable topography during this period, would give a preference for the model with thicker initial crust.

Model 3: Rise of a thermal plume

In this model, hot material (thermal mantle plume) arrives at the base of the lithosphere and replaces it in a variable thickness depending on plume temperature. We modeled temperature differences between 100 and 300 ºC, i.e. plume material at 1400 to 1600 °C. The temperature is maintained identical until 0.4 Ma (2.9 Ma in nature), then it relaxes. In order to achieve the desired total topographic uplift of about 400 m, the thickness of the plume material layer must vary between 25 km for a 1400 °C plume and 16 km for a 1600 °C plume. The effect is thus nearly linear with the temperature difference. However, subsidence is much more important for hotter

555 material. A simple model as presented here would therefore not be compatible with the
556 observations. Nevertheless, a continuous supply of hot material between 2.9 and 0.8 Ma ago would
557 maintain the topography at the observed height. We did not model the second pulse at 2.5 Ma (0.8
558 Ma in nature), since the other models show that the necessary topography variation can be easily
559 achieved.

560 For the quantitative interpretation, a critical condition is the one of local isostasy.
561 Significant elastic strength would reduce the topographic response. However, on the one hand, the
562 volcanism in Cape Verde indicates a locally hot and therefore weaker lithosphere. On the other
563 hand, especially for models 2 and 3, the structural variations used for the models are quite modest:
564 doubling crustal thickening or the thickness of the hot plume layer would certainly not be
565 exaggerated. It would be more difficult to consider much stronger thinning of the lithosphere in
566 Model 1 without the additional effect of hot rising plume material. Anyhow, also a combination of
567 all models would be able to explain the inferred uplift. The question now is application of the
568 model results to Santiago in the context of the archipelago and the Cape Verde Rise. Most large-
569 scale geophysical studies carried out in the Cape Verde Swell suggest that upwelling within the
570 asthenosphere supports the anomalous topography of the Cape Verde Swell, with minor
571 contributions from local thickened oceanic crust and, perhaps, partial thermal rejuvenation of the
572 lithospheric mantle. If large-scale swelling (dynamic uplift at the scale of the whole archipelago;
573 e.g. Huppert et al., 2020) were the mechanism responsible for island uplift , then one would expect
574 to find similar uplift in islands with similar age, which is not the case (e.g. Ramalho et al., 2010a, b,
575 c). Therefore, the solution to explain geological evidence should come from local mechanisms.
576 Model 1 is intended to simulate extension, which does not seem a sensible option in the
577 geodynamic setting of Cape Verde where rifting has never been recognized. In contrast, Model 3

looks like a good option, because this model simulates the scenario whereby the mantle plume dynamically uplifts the lithosphere underlying the Cape Verde Islands during Santiago's evolution, but is inconsistent with what is known about the differential vertical motion among the Cape Verde islands (e.g. Ramalho et al., 2010a, b, c), because some islands show large uplifts (e.g. Santiago and S. Nicolau), but other islands do not record uplift (e.g. Santo Antão and Fogo). Therefore, the large-scale plume (regional mechanism) cannot explain the differential uplift. The solution is therefore to look for a local mechanism, which is the case of magma underplating (Model 2), as already suggested to exist beneath the islands (e.g. Lodge and Helffrich, 2006; Ramalho et al., 2010b; Vinnik et al., 2012; Wilson et al., 2010).

7. Conclusions

We use paleoshorelines at different altitude and age to constrain the vertical motion history of Santiago Island. Specifically, we calculate the time-averaged vertical motion rates required to explain the present-day elevations of the dated sequence of paleoshorelines. We account for eustatic sea level changes and work progressively back in time to incorporate the more recent vertical motion rates implied by the youngest paleoshorelines into the vertical motion history of all older shorelines. We thus obtain a vertical motion history consisting of time-averaged vertical motion rates spanning the five intervening time periods between paleoshoreline formation and the present day: (1) > 6 Ma – this stage is certainly mostly submarine (seamount growth), but there is no consensus regarding the submarine or subaerial nature of the rocks of the Basement Complex currently cropping out onshore: all submarine, or subaerial in part? Did the seamount grow into an island with subaerial volcanism? (2) 5.06 to 3.29 Ma – given that all known rocks in this period are submarine, they can represent seamount growth or island subsidence. (3) 3.29 to 2.87 Ma – fast

601 uplift (0.96 mm/a) mostly responsible for putting submarine lavas currently close to 410 m altitude.
602 (4) 2.87 to 2.18 Ma – relatively fast subsidence (-0.11 mm/a), most likely due to the fast volcanic
603 growth of the most voluminous volcanic unit on the island, the Intermediate Volcanic Complex
604 (former Pico da Antónia Formation). (5) 2.18 to 0.811 Ma – stationary island (0.00 mm/a). (6)
605 0.811 to 0 Ma – relatively fast uplift (0.14 mm/a).

606 The advantage of using dated passage zones, at different ages (0.811, 2.18 and 2.87 Ma) and
607 in different places on the island, and a different procedure is that we find a more detailed history of
608 vertical motion consistent with geological observation. Instead of a simple general uplift at a
609 constant rate of ca. 0.092 mm/a (Ramalho et al., 2010a, b, c), our new data and methodology
610 indicate that Santiago experienced several periods of uplift, at different rates (0.95 to 0.14 mm/a),
611 intercalated with at least one period of subsidence (-0.11 mm/a).

612 We numerically tested top-down (volcanic loading) and bottom-up (lithosphere thinning,
613 underplating and mantle plume) mechanisms to explain the inferred vertical movements, and we
614 conclude that volcanic loading and crustal underplating are capable of producing the observed
615 subsidence and uplift, respectively.

616

617 **Acknowledgments**

618 This is a contribution to Project MEGAHazards2 (PTDC/GEO-GEO/0946/2014), funded by
619 FCT, Portugal. The sea level data used in this study was kindly supplied by Kenneth Miller, and
620 can be found here: https://www.ncdc.noaa.gov/paleo-search/study/13947. Thorough and
621 constructive reviews by five anonymous Reviewers helped to clarify and improve the quality of this
622 manuscript.

623

References

Afonso, J.C., Ranalli, G., Fernàndez, M., 2005. Thermal expansivity and elastic properties of the lithospheric mantle: results from mineral physics of composites. Phys. Earth Planet. Int. 149, 279-306. Doi: 10.1016/j.pepi.2004.10.003.

Ali, M. Y., A. B. Watts, & I. Hill, 2003. A seismic reflection profile study of lithospheric flexure in the vicinity of the Cape Verde Islands. J. Geophys. Res. 108, 2239, doi:10.1029/2002JB002155.

Bernard-Griffiths, J., Cantagrel, J.-M., Alves, C., Mendes, F., Serralheiro, A. & Macedo, J., 1975. Geochronologie: Donnés radiometriques potassium/argon sur quelques formations magmatiques des îlles de l'archipel du Cap Vert. Comptes Rendus des Seances de l'Academie des Sciences D280, 2429–2432.

Bintanja, R., van de Wal, R.S.W., Oerlemans, J., 2005. Modelled atmospheric temperatures and global sea levels over the past million years. Nature 437 (7055), 125–128.

Bonneville, A., Dosso, L., Hildenbrand, A., 2006. Temporal evolution and geochemical variability of the South Pacific superplume activity. Earth and Planetary Science Letters, 244(1-2):251-269.

Boulesteix, T., Hildenbrand, A., Gillot, P.Y., Soler, V., 2012. Eruptive response of oceanic islands to giant landslides: New insights from the geomorphologic evolution of the Teide–Pico Viejo volcanic complex (Tenerife, Canary). Geomorphology, 138 (1), 61-73.

Boulesteix, T., Hildenbrand, A., Soler, V., Quidelleur, X., Gillot, P.Y., 2013. Coeval giant landslides in the Canary Islands: Implications for global, regional and local triggers of giant flank collapses on oceanic volcanoes. Journal of Volcanology and Geothermal Research, 257, 90-98.

Carvalho, J., Bonadio, R., Silveira, G., Lebedev, S., Mata, J., Arroucau, P., s Meier, T., Celli, N.L., 2019. Evidence for high temperature in the upper mantle beneath Cape Verde archipelago from

Rayleigh-wave phase-velocity measurements. Tectonophysics 770, 228225.

Cas, R., & Wright, J., 1987. Volcanic successions. modern and ancient: a geological approach to processes, products and successions. London, UK: Chapman & Hall.

Costa, A.C.G., Marques, F.O., Hildenbrand, A., Sibrant, A.L.R., Catita, C.M.S., 2014. Large-scale catastrophic flank collapses in a steep volcanic ridge: the Pico-Faial Ridge, Azores Triple Junction. Journal of Volcanology and Geothermal Research, 272, 111-125.

Costa, A.C.G., Hildenbrand, A., Marques, F.O., Sibrant, A.L.R., Santos de Campos, A., 2015. Catastrophic flank collapses and slumping in Pico Island during the last 130 kyr (Pico-Faial ridge, Azores Triple Junction). J. Volcanol. Geotherm. Res., 302, 33-46.

Dash, B.P., Ball, M.M., King, G.A., Butler, L.W., Rona, P.A., 1976. Geophysical investigation of the Cape Verde archipelago. J. Geophys. Re. 81, 5249-5259.

de Boer, B., Van de Wal, R.S.W., Bintanja, R., Lourens, L.J., Tuetter, E., 2010. Cenozoic global ice-volume and temperature simulations with 1-D ice-sheet models forced by benthic δ18O records. Ann. Glaciol. 51, 23–33. Doi:10.3189/172756410791392736.

Germa, A., Quidelleur, X., Gillot, PY., Tchilinguirian, P., 2010. Volcanic evolution of the back-arc Pleistocene Payun Matru volcanic field (Argentina). Journal of South American Earth Sciences 29, 717-730.

Germa, A., Quidelleur, X., Lahitte, P., Labanieh, S. & Chauvel, C., 2011. The K–Ar Cassignol–Gillot technique applied to western Martinique lavas: a record of Lesser Antilles arc activity from 2 Ma to Mount Pelée volcanism. Quat. Geochronol. 6, 341–355.

Gillot, P. Y., Cornette, Y., 1986. The Cassignol technique for potassium–argon dating, precision and accuracy – examples from the Late Pleistocene to recent volcanics from southern Italy. Chem. Geol. 59, 205–222.

Gillot, P. Y., Cornette, Y., Max, N., Floris, B., 1992. Two reference materials, trachytes MDO-G and ISH-G, for argon dating (K–Ar and Ar-40/Ar-39) of Pleistocene and Holocene rocks. Geostandards Newsletter 16, 55–60.

Gillot, P. Y., Hildenbrand, A., Lefevre, J. C., Albore-Livadie, C., 2006. The K-Ar dating method: principle, analytical techniques and application to Holocene volcanic eruptions in Southern Italy. Acta Vulcanol. 18, 55–66.

Hansen, J., Sato, M., Russell, G., Kharecha, P., 2013. Climate sensitivity, sea level and atmospheric carbon dioxide. Phil Trans R Soc A 371: 20120294. Doi: 10.1098/rsta.2012.0294.

Hellfrich, G., Faria, B., Fonseca, J.F.B.D., Lodge, A., Kaneshima, S., Month, 2010. Transition zone structure under a stationary hot spot: Cape Verde. Earth Planet. Sci. Lett. 289, 156–161. https://doi.org/10.1016/j.epsl.2009.11.001.

Hess, J.C., and H. J. Lippolt. Compilation of K-Ar measurements on HD-B1 standard biotite. Phanerozoic Time Scale,.Bull. Liais. Inform. IUGS Subcomm. On Geochrono. Int. Geol. Correl. Program. Paris 12, 19-23 (1994).

Hildenbrand, A., Gillot, P.Y., 2006. Evidence for a differentiated ignimbritic activity ending the building-stage of Tahiti-Nui (French Polynesia). Comptes Rendus Geosciences 338, 280-287.

Hildenbrand, A., Gillot, P.Y., Soler, V., Lahitte, P., 2003. Evidence for a persistent uplifting of La Palma (Canary Islands) inferred from morphological and radiometric data, Earth Planetary Science Letters 210, 277-289.

Hildenbrand, A., Gillot, P.Y., Le Roy, I., 2004. Volcano-tectonic and geochemical evolution of an oceanic intra-plate volcano: Tahiti-Nui (French Polynesia). Earth Planetary Science Letters 217, 349-365.

Hildenbrand, A., Madureira, P., Marques, F.O., Cruz, I., Henry, B., Silva, P., 2008. Multi-stage

693 evolution of a sub-aerial volcanic ridge over the last 1.3 Myr: S. Jorge Island, Azores Triple
694 Junction. Earth and Planetary Science Letters 273, 289-298.
695 Hildenbrand, A., Marques, F.O., Costa, A.C.G., Sibrant, A.L.R., Silva, P.F., Henry, B., Miranda,
696 J.M., Madureira, P., 2012. Reconstructing the architectural evolution of volcanic islands from
697 combined K-Ar, morphologic, tectonic, and magnetic data: the Faial Island example (Azores).
698 Journal of Volcanology and Geothermal Research, 241-242, 39-48.
699 Hildenbrand A., Weis D., Madureira P., Marques F.O., 2014. Recent plate re-organization at the
700 Azores Triple Junction: evidence from combined geochemical and geochronological data on
701 Faial, S. Jorge and Terceira volcanic islands. Lithos 210-211, 27-39.
702 Hildenbrand, A., Marques, F.O., Catalão, J., 2018. Large-scale mass wasting on small volcanic
703 islands revealed by the study of Flores Island (Azores). Scientific Reports 8, 13898.
704 Holm, P.M., Grandvuinet, T., Friis, J., Wilson, J.R., Barker, A.K., Plesner, S., 2008. An ^{40}Ar-^{39}Ar
705 study of the Cape Verde hot spot: Temporal evolution in a semistationary plate environment. J.
706 Geophys. Res. 113, B08201, doi:10.1029/2007JB005339.
707 Huppert, K.L., Perron, J.T., & Royden, L.H. (2020). Hotspot swells and the lifespan of volcanic
708 ocean islands. Science Advances, 6(1), eaaw6906.
709 Huppert, K.L., Royden, L.H., Perron, J.T., 2015. Dominant influence of volcanic loading on
710 vertical motions of the Hawaiian Islands. Earth and Planetary Science Letters 418, 149-171.
711 Jones, J.G., 1969. Pillow lavas as depth indicators. American Journal of Science 267, 181–195.
712 Jones, J., & Nelson, P., 1970. The flow of basalt lava from air into water, its structural expression
713 and stratigraphic significance. Geological Magazine 107, 13–19.
714 Lachenbruch, A.H., Morgan, P., 1990. Continental extension, magmatism and elevation: Formal
715 relations and rules of thumb. Tectonophysics 174, 39-62.

716 Lodge, A., Helffrich, G., 2006. Depleted swell root beneath the Cape Verde Islands. Geology 34,
717 449–452.
718 Marques, F.O., Catalão, J.C., DeMets, C., Costa, A.C.G., Hildenbrand, A., 2013. GPS and tectonic
719 evidence for a diffuse plate boundary at the Azores Triple Junction. Earth and Planetary
720 Sciences Letters 381, 177-187.
721 Marques, F.O., Catalão, J.C., Hildenbrand, A., Costa, A.C.G., Dias, N.A., 2014. The 1998 Faial
722 earthquake, Azores: Evidence for a transform fault associated with the Nubia–Eurasia plate
723 boundary? Tectonophysics 633, 115-125.
724 Marques, F.O., Catalão, J.C., Hildenbrand, A., Madureira, P., 2015. Ground motion and tectonics in
725 the Terceira Island: Tectonomagmatic interactions in an oceanic rift (Terceira Rift, Azores
726 Triple Junction). Tectonophysics 651-652, 19-34.
727 Marques, F.O., Hildenbrand, A., Hübscher, C., 2018. Evolution of a volcanic island on the shoulder
728 of an oceanic rift and geodynamic implications: S. Jorge Island on the Terceira Rift, Azores
729 Triple Junction. Tectonophysics 738, 41-50.
730 McNutt, M., 1988. Thermal and mechanical properties of the Cape Verde Rise. J. Geophys. Res.
731 93, 2784–2794.
732 Miller, K.G., Kominz, M.A., Browning, J.V., Wright, J.D., Mountain, G.S., Katz, M.E., Sugarman,
733 P.J., Cramer, B.S., Christie-Blick, N., Pekar, S.F., 2005. The Phanerozoic record of global sea-
734 level change. Science 310, 1,293-1,298.
735 Miller, K.G., Mountain, G.S., Wright, J.D., Browning, J.V., 2011. A 180-million-year record of sea
736 level and ice volume variations from continental margin and deep-sea isotopic records.
737 Oceanography 24, 40–53.
738 Odin, G.S., 1982. Interlaboratory standards for dating purposes. *In:* Odin, G.S. (Ed.), Numerical

739 Dating in Stratigraphy. John Wiley and Sons, Chichester, pp. 123–150.
740 Pim, J., Watts, A.B., Grevemeyer, I., Krabbenhoeft, A., 2008. Crustal structure and origin of the
741 Cape Verde Rise. Earth Planet. Sci. Lett. 272, 422-428.
742 Porebski, S. & Gradzinski, R., 1990. Lava-fed Gilbert-type delta in the Polonez Cove Formation
743 (Lower Oligocene), King George Island, West Antarctica. In A. Colella, & D. Prior (Eds.),
744 Coarse Grained Deltas (vol. 10). International Association of Sedimentologists Special
745 Publication (pp. 335–351).
746 Quidelleur, X., Hildenbrand, A., Samper, A., 2008. Causal link between Quaternary paleoclimatic
747 changes and volcanic islands evolution. Geophysical Research Letters 35, L02303.
748 Rackzek, I., Stoll, B., Hofmann, A. W., Jochum, K.P., 2001. High-precision trace element data for
749 the USGS reference materials BCR-1, BCR-2, BHVO-1, BHVO-2, AGV-1, AGV-2, DTS-1,
750 DTS-2, GSP-1 and GSP-2 by ID-TIMS and MIC-SSMS. Geostandards Newsletter 25, 77-86.
751 Ramalho, R.S., Helffrich, G., Cosca, M., Vance, D., Hoffmann, D., Schmidt, D.N., 2010a. Vertical
752 movements of ocean island volcanoes: Insights from a stationary plate environment. Mar. Geol.
753 275, 84–95.
754 Ramalho, R., Helffrich, G., Cosca, M, Vance, D., Hoffmann, D., Schmidt, D.N., 2010b. Episodic
755 swell growth inferred from variable uplift of the Cape Verde hotspot islands. Nat. Geosc. 3, 774-
756 777.
757 Ramalho, R., Helffrich, G., Schmidt, D. N. & Vance, D., 2010c. Tracers of uplift and subsidence in
758 the Cape Verde Archipelago. J. Geol. Soc. Lond. 167, 519-538.
759 Ramalho, R. S., Quartau, R., Trenhaile, A. S., Mitchell, N. C., Woodroffe, C. D. & Avila, S. P.
760 (2013). Coastal evolution on volcanic oceanic islands: a complex interplay between volcanism,
761 erosion, sedimentation, sealevel change and biogenic production. Earth-Science Reviews, 127

140-170.

Ribeiro, L.P., Martins, S., Hildenbrand, A., Madureira, P., Mata, J., 2017. The genetic link between the Azores Archipelago and the Southern Azores Seamount Chain (SASC): The elemental, isotopic and chronological evidences. Lithos 294, 133-146.

Ricci, J., Quidelleur, X., Lahitte, P., 2015. Volcanic evolution of central Basse-Terre Island revisited on the basis of new geochronology and geomorphology data. Bull. Volcanol. 77, 84, DOI: 10.1007/s00445-015-0970-7.

Ricci, J., Quidelleur, X., Pallares, C., Lahitte, P., 2017. High-resolution K-Ar dating of a complex magmatic system: The example of Basse-Terre Island (French West Indies). J. Volcanol. Geotherm. Res. 345, 142-160.

Robertson, E.C., 1988. Thermal properties of rocks. USGS Open-File Report 88-441, Reston, VA, 110 pp.

Salvany, T., Lahitte, P., Nativel, P., Gillot, P.-Y., 2012. Geomorphic evolution of the Piton des Neiges volcano (Réunion Island, Indian Ocean): competition between volcanic construction and erosion since 1.4 Ma. Geomorphology 136, 132-147.

Serralheiro A., 1976. A Geologia da ilha de Santiago (Cabo Verde). Bol. Museu Lab. Mineral. Geol. Fac. Ciências Lisboa 14.

Sibrant, A., Marques, FO., Hildenbrand, A., 2014. Construction and destruction of a volcanic island developed inside an oceanic rift: Graciosa Island, Terceira Rift, Azores". J. Volcanol. Geotherm. Res. 284, 32-45.

Sibrant, A.L.R., Hildenbrand, A., Marques, FO., Weiss, B., Boulesteix, T., Hübscher, C., Lüdmann, T., Costa, A.C.G., Catalão, J.C., 2015. Morpho-structural evolution of a volcanic island developed inside an active oceanic rift: S. Miguel Island (Terceira Rift, Azores). J. Volcanol.

785 Geotherm. Res. 301, 90-106.
786 Sibrant, A.L.R., Hildenbrand, A., Marques, F.O., Costa, A.C.G., 2015. Volcano-tectonic evolution
787 of the Santa Maria Island (Azores): Implications for paleostress evolution at the western
788 Eurasia–Nubia plate boundary. J. Volcanol. Geotherm. Res. 291, 49-62.
789 Silva, P.F., Henry, B., Marques, F.O., Hildenbrand, A., Madureira, P., Mériaux, C.A., Kratinová,
790 Z., 2012. Palaeomagnetic study of a subaerial volcanic ridge (São Jorge Island, Azores) for the
791 past 1.3 Myr: evidence for the Cobb Mountain Subchron, volcano flank instability and
792 tectonomagmatic implications. Geophysical Journal International 188, 959-978.
793 Silva, P.F., Henry, B., Marques, F.O., Hildenbrand, A., Lopes, A., Madureira, P., Madeira, J.,
794 Nunes, J.C., Roxerová, Z., 2018. Volcano-tectonic evolution of a linear volcanic ridge (Pico-
795 Faial Ridge, Azores Triple Junction) assessed by paleomagnetic studies. J. Volcanol. Geotherm.
796 Res. 352, 78-91.
797 Steiger, R.H., Jager, E., 1977. Subcommission on geochronology: convention on the use of decay
798 constants in geo and cosmochronology. Earth Planet. Sci. Lett. 36, 359–362.
799 Schwarz, W.H., Trieloff, M., 2007. Intercalibration of 40Ar–39Ar age standards NL-25, HB3gr
800 hornblende, GA1550, SB-3, HD-B1 biotite and BMus/2 muscovite. Chemical Geology 242,
801 218-231.
802 Vinnik, L., Silveira, G., Kiselev, S., Farra, V., Weber, M., Stutzmann, E., Month, 2012. Cape Verde
803 hotspot from the upper crust to the top of the lower mantle. Earth Planet. Sci. Lett. 319–320,
804 259–268. https://doi.org/10.1016/j.epsl.2011.12.017.
805 Wilson, D., Peirce, C., Watts, A., Grevemeyer, I., Krabbenhöft, A., 2010. Uplift at lithospheric
806 swells I: seismic and gravity constraints on the crust and uppermost mantle structure of the cape
807 verde mid-plate swell. Geophys. J. Int. 182, 531–550. https://doi.org/10.1111/j.1365-

246X.2010.04641.x.

Wilson, D., Peirce, C., Watts, A., Grevemeyer, I., 2013. Uplift at lithospheric swells II: is the Cape Verde mid-plate swell supported by a lithosphere of varying mechanical strength? Geophys. J. Int. 193, 798–819. https://doi.org/10.1093/gji/ggt034.